Cement and Concrete Composites 135 (2023) 104816

Contents lists available at ScienceDirect

Cement and Concrete Composites

journal homepage: www.elsevier.com/locate/cemconcomp

Sunlight to heal mortar cracks: Photocatalytic self-healing mortar

Yiming Zhou [a,b], Mohamed Elchalakani [b,**], Peng Du [a,*], Chuanzhi Sun [c], Zuhua Zhang [d,e], Hao Wang [e]

[a] Shandong Provincial Key Laboratory of Preparation and Measurement of Building Materials, University of Jinan, Jinan, 250022, PR China
[b] School of Civil, Environmental and Mining Engineering, University of Western Australia, WA, 6009, Australia
[c] College of Chemistry, Chemical Engineering and Materials Science, Collaborative Innovation Center of Functionalized Probes for Chemical Imaging in Universities of Shandong, Shandong Provincial Key Laboratory of Clean Production of Fine Chemicals, Institute of Materials and Clean Energy, Shandong Normal University, Jinan, 250014, PR China
[d] Hunan Univ, Coll Civil Engn, Key Lab Green & Adv Civil Engn Mat & Applicat Tec, Changsha, 410082, Hunan, PR China
[e] University of Southern Queensland, Center for Future Materials, Toowoomba, Qld, 4350, Australia

ARTICLE INFO

Keywords:
Self-healing
Mortar
Sunlight
Photocatalysis
Capsules

ABSTRACT

Using capsules containing repairing materials to heal concrete cracks has always been a method of great interest to achieve self-healing concrete. Breaking the capsules to release repairing materials is a challenging task. The current methods used to break capsules mainly rely on instant external forces, which implies that slowly developing cracks cannot be healed by capsules. In this paper, we present a novel photocatalytic self-healing mortar to solve this problem. To do so, $NaHCO_3$, $Ca(OH)_2$ and citric acid are inserted into macro capsules. Then, the photocatalyst TiO_2 is added to the insoluble shells of capsules to allow them to be broken by sunlight. After shells of capsules are degraded by sunlight, $NaHCO_3$, $Ca(OH)_2$ and citric acid react in a wet environment to generate repairing materials that fill the cracks. To support the feasibility of the idea, physical and chemical experiments and characterization studies were conducted. Two-millimetre wide mortar cracks can be healed by the substances released from the photocatalytic capsules. The results of water permeability tests show that the two photocatalytic capsules can reach 52% healing efficiency. The characterization results show that the substances filling the cracks are unreacted $NaHCO_3$, $Ca(OH)_2$, citric acid and insoluble products of calcium salts. Our results suggest that sunlight can be used for the self-healing of mortar.

1. Introduction

Owing to deformation, creep, fatigue, drying shrinkage, freeze–thaw cycles, etc., concrete structures inevitably develop cracks [1–6]. These cracks not only decrease the strength of concrete structures but also provide access for corrosive substances in the environment to penetrate into the concrete [7,8]. Therefore, repairing cracked concrete structures is always a research topic in the fields of concrete and mortar materials. Among numerous methods of repairing concrete or mortar cracks, such as bacteria, super absorbent polymers and wet carbonation [9–13], much attention has been given to using capsules to heal concrete cracks [14–16]. Using capsules to heal concrete cracks is a self-healing method. Usually, researchers give the capsules the capacity to heal the cracks by adding repairing materials to the capsules [16,17]. When cracks develop, the capsules break, and the repairing materials are released to heal the cracks. According to related studies, the repairing materials mainly consist of cyanoacrylates [18], polyurethane [15], epoxy [17], silicons, hydrogels [19] or alkali-silica solutions [20]. However, there is still an unresolved problem where capsules do not always rupture with the advent of cracks [17,21]. The rupture of capsules only occurs when capsules receive a large degree of impact. Apparently, some types of cracks cannot achieve the above condition. For example, the cracks caused by the long-term creep of concrete can hardly lead to the rupture of capsules [22,23]. To solve this problem, several ideas have been put forward, such as using more brittle capsules or strengthening the bond between capsules and concrete. Blaiszik [24] reported a method to produce microcapsules with a shell wall thickness of 77 nm. However, nanosized capsules cannot heal visible cracks beyond the serviceability limit. Thao et al. [25] found that glass tubes are easily ruptured, so they used them to contain repairing materials. Although such a fragile

* Corresponding author.
** Corresponding author.
E-mail addresses: mohamed.elchalakani@uwa.edu.au (M. Elchalakani), mse_dup@ujn.edu.cn (P. Du).

https://doi.org/10.1016/j.cemconcomp.2022.104816
Received 4 July 2022; Received in revised form 17 September 2022; Accepted 16 October 2022
Available online 27 October 2022

material is easy to break, it is inconvenient in the construction process. In fact, either using vulnerable materials or making the capsules thinner has been the main focus of scholars in most studies. To the best of our knowledge, very little research effort has been directed to the external factor leading to the breakage of capsules.

In this study, we proposed a new method for using capsules to heal mortar cracks: photocatalytic self-healing capsules. The photocatalytic effect [26–28], as a new technology for utilizing light energy, has attracted much attention in recent years. The photocatalytic effect is defined as the catalytic oxidation reaction of photocatalysts under light, also known as photocatalysis. Photocatalysis can achieve many functions, such as hydrogen production [29,30], air purification [31,32], and degradation of dyes and antibiotics [33–38]. These functions can be achieved only by sunlight. Thus, we propose a novel idea where photocatalysts can be added to the cover of capsules so that the capsules break with the appearance of cracks. Specifically, when cracks appear on the surface of concrete, sunlight immediately penetrates the interior of concrete, which promotes the rupture of capsules with the help of photocatalysts in the capsule shells. In this paper, we use polyethene (PE) materials and the photocatalyst TiO_2 to create the shell of capsules and insert $NaHCO_3$, $Ca(OH)_2$ and citric acid inside the capsules. In addition, the PE materials come from plastic waste bottles. Under sunlight, TiO_2 degrades PE materials [39–41], which can lead to the ruptures of capsules. Furthermore, $NaHCO_3$, $Ca(OH)_2$ and citric acid in the capsules reacts to generate repairing materials to fill the cracks when encountering rain water.

The novel aspect of this study involves the use of sunlight for the first time for the self-healing of mortar. To verify the feasibility of the proposed method, the self-healing process is implemented through experiments.

2. Materials and methods

2.1. Materials

PE (polyethylene) was obtained from waste PE bottles. $NaHCO_3$ and $Ca(OH)_2$ (purity 99.99%) were obtained from Aladdin Co. Ltd. (Shanghai, China). TiO_2 nanopowder (rutile, ≥99%) was purchased from Macklin Inc. (Macklin, Shanghai, China). Ordinary Portland cement (P.O 42.5), ISO standard sands (ISO 679:2009, quartz sands) and deionized water were used to produce the mortar specimens. Ordinary Portland cement was purchased from China Resources Cement Holdings Limited. The ISO standard sand was purchased from Xiamen Iso Standard Sand Co., Ltd. The ratio of cement, sand and water is 1:3:0.5. The chemical and mineral compositions of the cement are shown in Table 1.

2.2. Healing mechanism

Fig. 1 shows a schematic of the self-healing mechanism applied in this study. The self-healing capsules filled with $NaHCO_3$, $Ca(OH)_2$ and citric acid are first embedded in mortar, as shown in step (1) in Fig. 1. Once cracks form in the mortar, sunlight can penetrate the mortar, and the capsule shell (cover) that is located on the path of crack propagation can contact sunlight. The shell of capsules is made by the PE material photocatalyst TiO_2. TiO_2 can absorb sunlight and gradually degrade the PE material, which results in the rupture of capsules after a long period of time, followed by exposure of the healing agent $NaHCO_3$, $Ca(OH)_2$ and citric acid in the capsules, as shown in step (2). When the cracked area is exposed to water (by rain or other means, such as step (3)), $NaHCO_3$ reacts with citric acid to transiently produce CO_2 bubbles (as shown in Eq. (1)).

$$3NaHCO_3 + C_6H_8O_7 = Na_3C_6H_5O_7 + 3H_2O + 3CO_2\uparrow \quad (1)$$

The bubbles can push $NaHCO_3$, $Ca(OH)_2$ and water to fill the cracks. Some possible reactions also occur at the same time.

$$NaHCO_3 + Ca(OH)_2 = NaOH + CaCO_3\downarrow + H_2O \quad (2)$$

$$2NaHCO_3 + Ca(OH)_2 = Na_2CO_3 + CaCO_3\downarrow + 2H_2O \quad (3)$$

$$2C_6H_8O_7 + Ca(OH)_2 = Ca_3(C_6H_5O_7)_2\downarrow + 2H_2O \quad (4)$$

If the situation in which products react with initial reactants is considered, the chemical reaction equations below will occur.

$$C_6H_8O_7 + 3NaOH = Na_3C_6H_8O_7 + 3H_2O \quad (5)$$

$$3Na_2CO_3 + 2C_6H_8O_7 = Na_3C_6H_5O_7 + 3H_2O + 3CO_2\uparrow \quad (6)$$

$$Ca(OH)_2 + CO_2 = CaCO_3\downarrow + H_2O \quad (7)$$

$$Ca(OH)_2 + 2CO_2 = Ca(HCO_3)_2 \quad (8)$$

As seen in Eqs. (1)–(8), insoluble $CaCO_3$ and $Ca_3(C_6H_5O_7)_2$ are generated, which can fill (seal) the cracks. $CaCO_3$ has been demonstrated to repair mortar cracks in many studies [42–45]. However, $Ca_3(C_6H_5O_7)_2$ has not been used as a repairing material in self-healing concrete or mortar materials. Considering the conditions above, we compare [46] $CaCO_3$ and $Ca_3(C_6H_5O_7)_2$ (as shown in Table 2) to show that $Ca_3(C_6H_5O_7)_2$ can also be a repairing material.

Table 2 shows that although the solubility value of $Ca_3(C_6H_5O_7)_2$ is higher than that of $CaCO_3$, the solubilities of $Ca_3(C_6H_5O_7)_2$ and $CaCO_3$ are of the same order of magnitude. The reason $CaCO_3$ could be a repairing material is largely due to its insolubility [47–50]. According to the relevant definition [51], $Ca_3(C_6H_5O_7)_2$ and $CaCO_3$ are very slightly soluble in water. Therefore, $Ca_3(C_6H_5O_7)_2$ could also be the repairing material but may not be as good as $CaCO_3$.

Meanwhile, of course, some side reaction products are also formed by Eqs. (1)–(8). In fact, Eqs. (1)–(8) are our conjecture based on the principle of chemical reactions [52]. Since the reaction in Eqs. (1)–(8) are not performed in solution forms, it is difficult to clearly state which are the main chemical reactions of Eqs. (1)–(8) and whether such chemical reactions are performed completely. However, the self-healing property will be achieved as long as sufficient repairing materials are created. Therefore, we decided to focus this study on explaining the generated products clearly filling (sealing) the cracks.

The reasons to choose citric acid as the acid to react with $NaHCO_3$ mainly come from the considerations of economy, applicability, and safety. Theoretically, most acids can react with citric acid to generate many bubbles, whereas four conditions need to be ensured: (1) solid acid; (2) safe to operate; (3) inexpensive and (4) no pollution. Among the numerous acids, citric acid meets the conditions, so citric acid is selected.

2.3. Preparation of photocatalytic capsules filled with $NaHCO_3$, $Ca(OH)_2$ and citric acid

The preparation of the photocatalytic capsules involves three steps. Fig. 2 shows the whole encapsulation process.

In the first step, $NaHCO_3$, $Ca(OH)_2$, $C_6H_8O_7$ (citric acid) and water were mixed and put into spherical forming moulds. The inside diameter of the forming mould is approximately 8 mm. The molar ratio of

Table 1
Chemical and mineral compositions of the cement.

CaO	SiO_2	Al_2O_3	Fe_2O_3	MgO	SO_3	Na_2O	P_2O_5	MnO	f-CaO
57.31%	22.64%	7.06%	3.33%	3.21%	2.35%	0.19%	0.21%	0.13%	1.32%

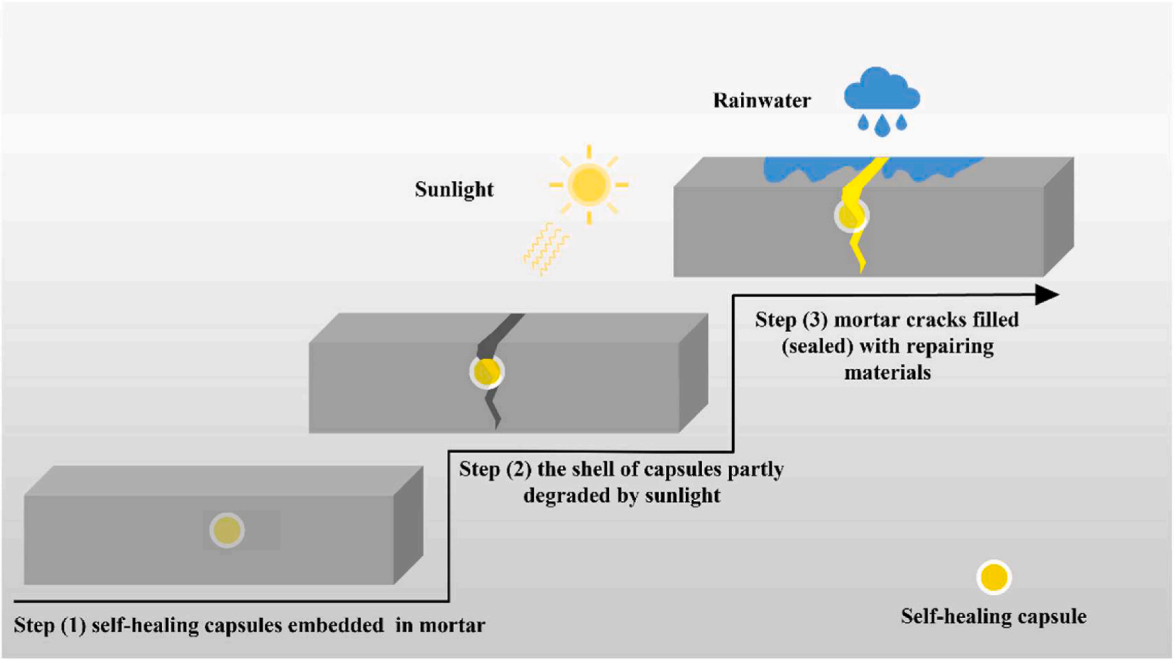

Fig. 1. Schematic of the working mechanism of the self-healing system.

Table 2
Comparison between $CaCO_3$ and $Ca_3(C_6H_5O_7)_2$.

	$CaCO_3$	$Ca_3(C_6H_5O_7)_2$
Solubility in water	0.013 g/L (25 °C)	0.095 g/L (25 °C)
Solubility product (*K*sp)	3.3×10^{-9}	/
Acidity (p*K*a)	9.0	/

Note: Ksp and p*K*a are the solubility product constant and acid dissociation constant, respectively.

$NaHCO_3$, $Ca(OH)_2$, $C_6H_8O_7$ and water was 200:100:200:1. A small amount of water was added to $NaHCO_3$, $Ca(OH)_2$ and $C_6H_8O_7$ to generate cohesive force to mould $NaHCO_3$, $Ca(OH)_2$ and $C_6H_8O_7$ well. There was a weak reaction when $NaHCO_3$, $Ca(OH)_2$, $C_6H_8O_7$ and 0.5 ml deionized water were mixed. The weak reaction generated viscosity among $NaHCO_3$, $Ca(OH)_2$, and $C_6H_8O_7$ [53]. The viscosity could make $NaHCO_3$, $Ca(OH)_2$ and $C_6H_8O_7$ keep their shape outside of the spherical moulds. Note that only a small amount of water was used in this step. Too much water will result in significant reactions of $NaHCO_3$, $Ca(OH)_2$ and $C_6H_8O_7$ in advance. After 72 h, the spherical mixture was removed from the mould (as shown in Fig. 3(a)). The second step is to make the shell for the spherical mixture. The shell of the photocatalytic self-healing capsule needs to be degraded under sunlight. Thus, we need to use materials that can be degraded by photocatalysts to make suitable shells of self-healing capsules. For photocatalysts, many types of photocatalysts of different chemistries are available for selection, such as g-C_3N_4, $BiPO_4$, $BiVO_4$, and TiO_2 [54]. Different types of photocatalysts have different features. In this study, the photocatalyst needed should have two features since the photocatalyst will be applied in construction materials. First, photocatalysts must be nontoxic and pollution-free, which means photocatalysts such as $BiPO_4$ and $BiVO_4$ cannot be used in this study [55]. Second, photocatalysts should have the significant advantage of being readily available and inexpensive, which means that the process is practical and can be applied on a large scale. Based on the description above, we selected TiO_2, which is currently the most widely used photocatalyst in the world and has a low cost [56]. For materials that can be degraded by photocatalysts, we selected PE materials considering their advantages of being nontoxic, pollution-free and waterproof. In the last step, we heated PE waste bottles (cut into pieces of approximately 2 cm) in beakers through an oil bath until they melted and then put the spherical mixture and TiO_2 into beakers. After stirring for 1 min, the spherical mixture was removed. The PE material quickly solidified at room temperature and formed a shell on the surface of the globular mixture. TiO_2 also existed in the shell. To date, photocatalytic self-healing capsules have been successfully prepared and are shown in Fig. 3(b), and six capsules were made. As shown in Fig. 3(b), there are

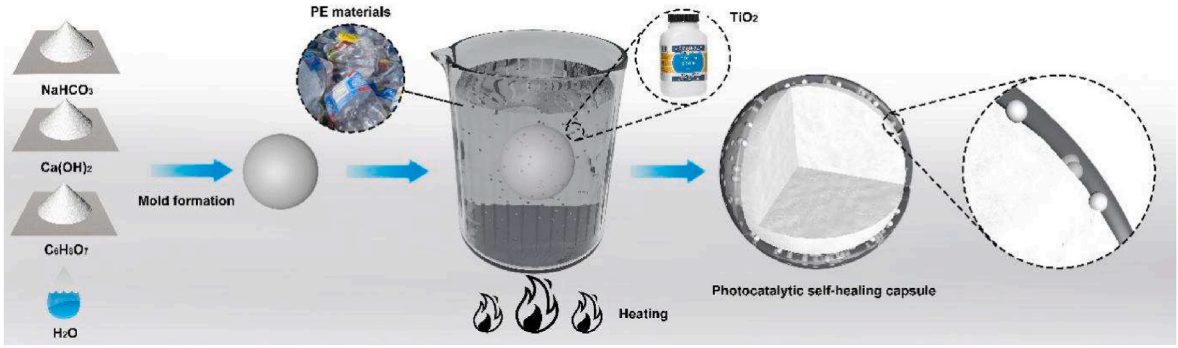

Fig. 2. Entire fabrication procedure for photocatalytic capsules.

Fig. 3. (a) Spherical mixture of $NaHCO_3$, $Ca(OH)_2$ and $C_6H_8O_7$ and (b) photocatalytic self-healing capsules.

indentations on the surface of the capsules. This was possibly caused by the uneven shrinkage of PE materials at room temperature [57]. Finally, the PE shell thickness and weight were measured. The PE shell thickness was obtained by the difference between the diameters of the spherical mixture of $NaHCO_3$, $Ca(OH)_2$ and $C_6H_8O_7$ and photocatalytic self-healing capsules. The diameter was defined as the average value in ten different directions. According to the measurement results, the average diameter of the six spherical mixtures is 8 mm, and the average diameter of the six photocatalytic capsules is 8.4 mm. Thus, the thickness of the PE shell is approximately 0.2 mm. The average weight of the six photocatalytic capsules is 6.9 g.

2.4. Feasibility analysis of photocatalytic capsules to protect the repairing agent and rupture under sunlight

2.4.1. Ability of photocatalytic capsules to retain/protect the repairing agent

The photocatalytic capsules need to survive before contacting sunlight. It is well known that PE materials are insoluble [58]; thus, photocatalytic capsules are theoretically waterproof. However, the addition of TiO_2 to the capsule shell may influence the waterproof property of capsules. Thus, we need to determine whether the photocatalytic capsules are able to retain/protect the repairing agent. Before cracks appear, the most likely factor causing the breakage of photocatalytic capsules is water infiltration into the mortar. According to related studies, the hydraulic pressure coming from the water that infiltrated the mortar is too small to damage PE materials [59,60]. Therefore, the effects of water immersion on the photocatalytic capsules were studied. The waterproof capacity of the photocatalytic capsules was evaluated by immersing the capsule in water. After a period of immersion (2 h, 4 h, 6 h and 8 h), the capsules were removed, and the survival of capsules was evaluated by the mass loss rate. The mass loss rate is defined as Formula (9).

$$\text{Mass loss rate} = \eta = \frac{Mass_a - Mass_b}{Mass_a} \tag{9}$$

where $Mass_a$ is the mass of capsules before immersion and $Mass_b$ is the mass of capsules after immersion. If the mass loss rate does not change after some time, the photocatalytic capsules will not be dissolved by water in practical applications. The testing results are listed in Table 3. The photocatalytic capsules only lost some weight in the first 4 h, possibly because a very small amount of TiO_2 on the surface dissolved in water. The results show that the photocatalytic capsules are suitable for application in self-healing as they are waterproof.

Table 3
Results of the survival test on the capsules prepared in water.

Time	Mass loss rate
2 h	0.7%
4 h	0.9%
6 h	0.9%
8 h	0.9%

2.4.2. Capsule rupture under sunlight

The rupture of PE shells of photocatalytic capsules under sunlight is a prerequisite to obtain the self-healing function in mortar. To prove the feasibility of applying the prepared capsules in mortar, cracked mortar specimens with embedded photocatalytic capsules were placed under simulated sunlight. The photocatalytic degradation of PE has already been extensively studied [39,61], so we focus on using photocatalysis technology to achieve self-healing in this study rather than researching the degradation mechanism of capsules. Therefore, we briefly discuss the degradation mechanism of PE material based on related references. The photocatalytic degradation of PE materials is a complex process, as discussed below. TiO_2 particles absorb light to generate mobile electrons and holes in the conduction and valence bands, respectively (Eq. (10)) [61]. Subsequently, reactions with O_2 lead to the formation of several reactive oxygen species, such as $O_2^{\bullet-}$, $HO_2^{\bullet}$ and $HO^{\bullet}$ (Eq. (11)–(16)). These active oxygen species initiate the degradation reaction by attacking neighbouring polymer chains (Eq. (17)). Meanwhile, the degradation process spatially extends into the polymer matrix through the diffusion of the reactive oxygen species. When the carbon-centred radicals enter the polymer chain, their successive reactions trigger chain cleavage with oxygen incorporation, and groups with more sample structures are produced (as shown in Eqs. 18–21). Finally, Equation (22) indicates that PE materials are mainly photocatalytically oxidized to CO_2 and H_2O under the action of reactive oxygen species.

$$TiO_2 \xrightarrow{hv} TiO_2(e^- + h^+) \tag{10}$$

$$O_{2(ads)} + e^- \rightarrow O_2^{\bullet-} \tag{11}$$

$$O_2^{\bullet-} + H_2O \rightarrow HO_2^{\bullet} + OH^- \tag{12}$$

$$2HO_2^{\bullet} \rightarrow H_2O_2 + O2 \tag{13}$$

$$H_2O_2 + hv \rightarrow 2^{\bullet}OH \tag{14}$$

$$OH^- + h^+ \rightarrow {}^{\bullet}O\,H \tag{15}$$

$$H_2O_{ads} + h^+ \rightarrow {}^{\bullet}O\,H + H^+ \tag{16}$$

$$-(CH_2CH_2)- + {}^{\bullet}O\,H \rightarrow -\left(\dot{C}\,HCH_2\right)- + H_2O \tag{17}$$

$$-\left(\dot{C}HCH_2\right)- + O_2 \rightarrow -\left(\dot{C}H(OO)CH_2\right)- \tag{18}$$

$$-(\mathrm{CH}(\dot{\mathrm{O}}\,\mathrm{O})\mathrm{CH_2})- + -(\mathrm{CH_2CH_2})- \rightarrow -(\mathrm{CH(OOH)CH_2})- + -(\mathrm{CH_2\dot{C}H})- \quad (19)$$

$$-(\mathrm{CH(OOH)CH_2})- + h\nu \rightarrow -(\mathrm{CH}\,\dot{\mathrm{O}}\;\mathrm{CH_2})- + \dot{\mathrm{O}}\mathrm{H} \quad (20)$$

$$-(\mathrm{CH\dot{O}\,CH_2})- \rightarrow -{}^{\bullet}\mathrm{CHO} + \mathrm{C\ H_2CH_2}- \quad (21)$$

$${}^{\bullet}\mathrm{CH_2CH_2} - + \mathrm{O_2} \xrightarrow{\mathrm{TiO_2},\, h\nu} \text{intermediates such as carboxylic acids, carboxylates, ketones and aldehydes} \rightarrow \mathrm{H_2O} + \mathrm{CO_2}\,(\text{evolution}) \quad (22)$$

where $h\nu$ in Eqs. (10), (14) and (20) represents photon energy; "ads" in Eqs. (11) and (16) represents the absorbent; and h^+ represents electron holes.

Related studies have reported that a greater degree of photocatalytic degradation of PE materials requires approximately 100 ~ 300 h [41,

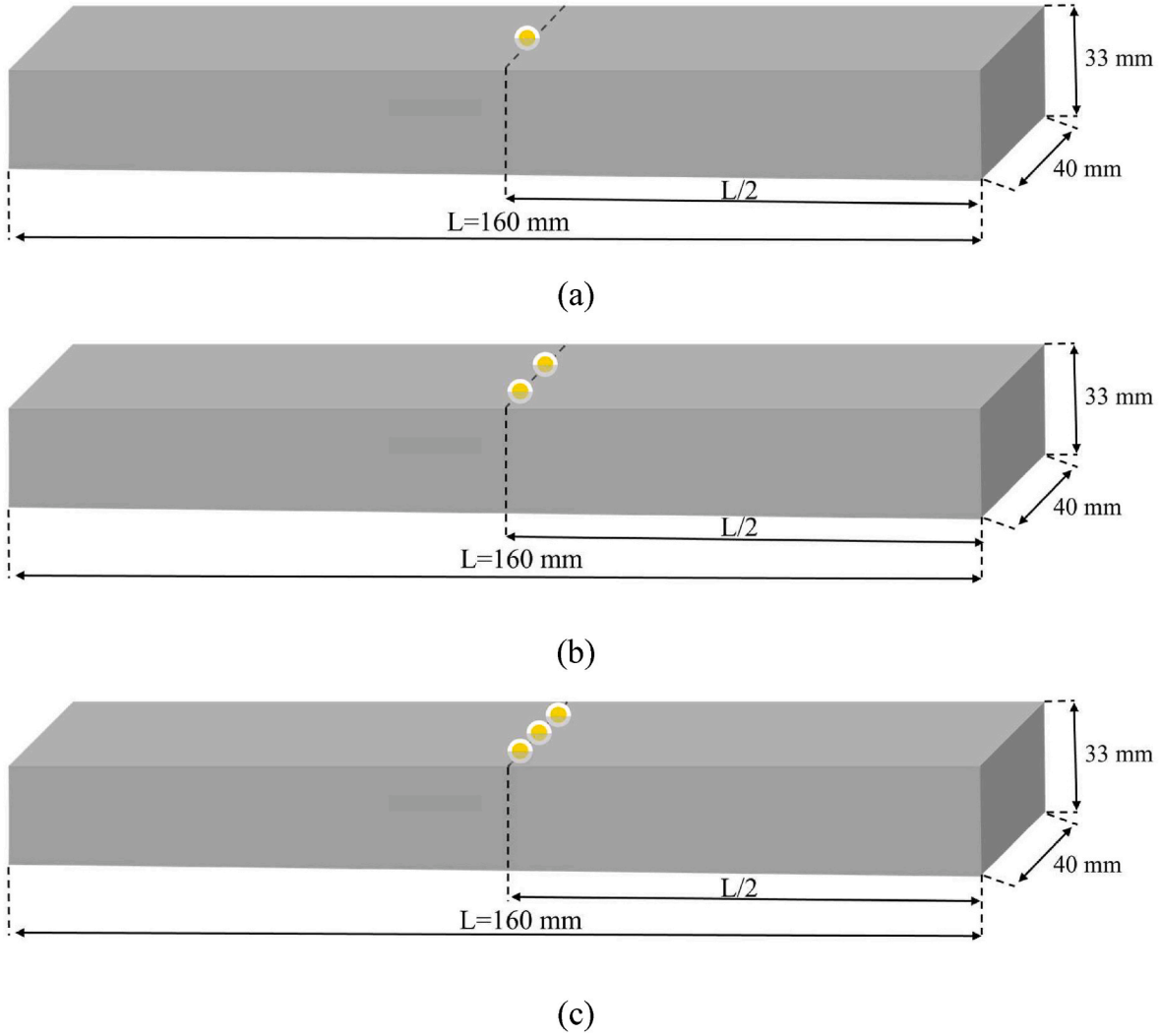

Fig. 4. Locations of capsules in the sample.

62–65]. Thus, the irradiation time is conservatively chosen to be 100 h.

2.5. Cracked sample preparation

2.5.1. Width of cracks

Since the rupture of photocatalytic self-healing capsules is caused by sunlight, the photocatalytic self-healing capsules inside the samples need to receive enough sunlight. Therefore, we need to find an appropriate width of cracks to conduct experiments. According to related studies [66–68], the width of mortar cracks that can be healed by capsules and the width of the capsules are within the same order of magnitude. In other words, capsules can only heal cracks that have similar sizes. In this study, the diameter of the photocatalytic self-healing capsules was approximately 8 mm. In addition, Nama et al. [69] conducted surveys on the width of nonstructural cracks of concrete and mortar structures and found that the width of nonstructural cracks could be divided into three types, as follows, with medium-sized cracks being the most common.

(1) Thin – less than 1 mm in width
(2) Medium – 1 mm–2 mm in width
(3) Wide – more than 2 mm in width

To make this study more practical, 2 mm was chosen as the width of cracks in this study.

2.5.2. Depth of cracks

For the depth of nonstructural cracks, Barve et al. [70] conducted a case study on the depth of nonstructural concrete cracks. The case study shows that the depth of most nonstructural cracks is distributed between 1 mm and 7 mm. Therefore, 7 mm was selected as the depth of cracks.

2.5.3. Sample preparation

Three prism samples (40 mm × 40 mm × 160 mm) were used in this study. First, a layer of 33 mm mortar was poured into moulds, and the moulds were vibrated for 1 min. Then, one, two, and three photocatalytic capsules were placed in the middle of the three moulds (as shown in Fig. 4). The capsules would be partly immersed in unhardened mortar due to gravity but remained stationary under the effect of friction between capsules and mortar after seconds. After positioning the photocatalytic capsules, the moulds were filled with mortar. In this way, the distances between the capsules and the top surfaces of the samples were controlled at approximately 7 mm. Considering the diameter of capsules, the actual distance from the surfaces of capsules to the top surfaces of mortar should be smaller than 7 mm to ensure that the capsules were able to be exposed when 7 mm-deep cracks were created.

After casting, the samples were wrapped with plastic film and stored under normal curing conditions (20 °C, >95% RH) for 24 h. Subsequently, the samples were cured at room temperature for another 21 days. Thus, three prism samples containing one, two, and three capsules were prepared.

2.6. Crack creation

Since the photocatalytic capsules were located in the middle of the samples, the cracks needed to be introduced to the middle of the samples to expose the capsules to sunlight. Thus, we conducted a three-point bending test on the samples to create cracks. The load was applied at a uniform speed of 0.2 mm/min through a microcomputer-controlled electronic universal testing machine (CDT1305-2, MTS Industrial Systems Co., Inc., Shenzhen, China). Once the cracks developed, loading was stopped. The samples were immediately split into two halves when cracks developed, which means that the width of cracks obtained by the process above can be adjusted by changing the distance between the two blocks. Thus, we adjusted the distance between fractured mortar blocks to make the width of cracks 2 mm (as shown in Fig. 5(a)). Note that the cracks go through the samples (the two mortar blocks were separated) when crack widths were set. In addition, the samples were kept in moulds during any movement to retain the 2 mm crack width.

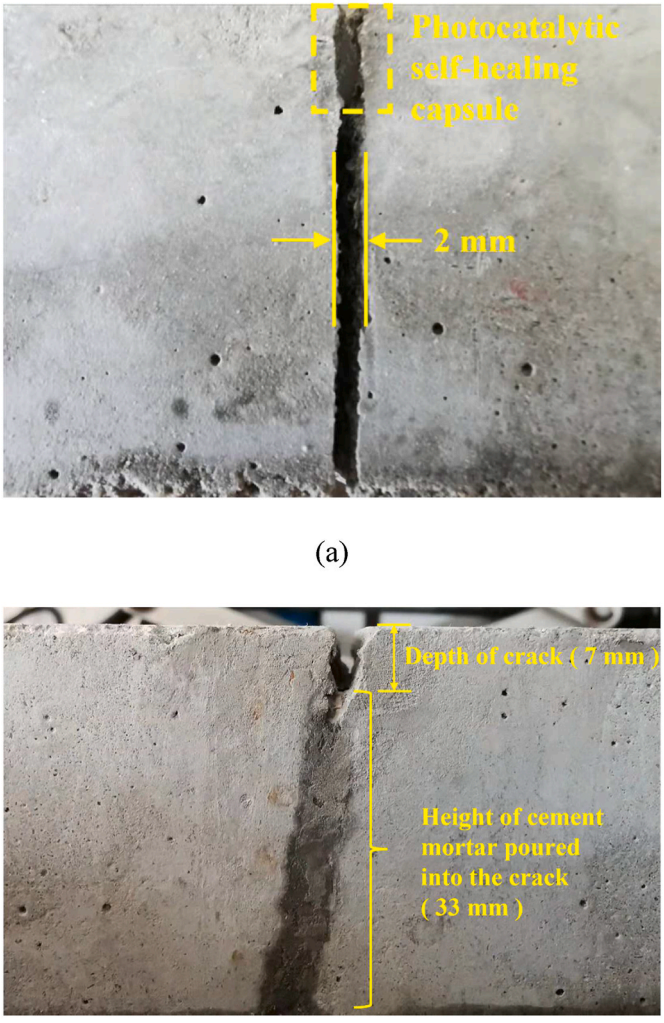

Fig. 5. (a) Top view showing the width of cracks of 2 mm and (b) side view showing the depth of cracks of 7 mm.

To achieve the specific depth of cracks, the following procedures were performed. The cracked mortar samples were put into the mould while keeping the crack width unchanged. Then, the cement mortar was poured into the cracks until the distance between the top face of the mortar and the top of the cracks reached 7 mm. Finally, the samples were cured again for 21 days. Fig. 5(b) shows the cracks only one day after the cement mortar was partially poured into the cracks. As shown in Fig. 5(b), the colour of the cement mortar poured into the cracks is much deeper than that of the samples owing to the shorter hydration time.

2.7. Irradiation process

The purpose of irradiation is to let the photocatalyst TiO_2 degrade the PE capsule shell. There have been numerous experimental studies on the degradation of PE by TiO_2, and the irradiation process can be designed by referencing the related studies. For the irradiation time, Zhao et al. [63] conducted similar experiments, degrading PE film by TiO_2 under sunlight. According to Ref. [59], the weight loss of the PE-TiO_2 (1 wt%) film reached 42% under solar irradiation for 300 h.

Fig. 6. Irradiation directed to the concrete cracks.

Because the mass ratio of PE and TiO_2 was 6:4 when the capsules shells were made, the irradiation time of this study was assumed to be much shorter than 300 h. Thus, the irradiation time was set to 100 h. Because the mortar cracks investigated in this study were thought to be caused by ageing and creep and did not require immediate repair, 100 h was considered to be acceptable. For the light source, a 500 W xenon lamp (Beijing China Education Au-light Co., Ltd., China) with an AM1.5 daylight optical filter was selected since the light from the xenon lamp is very similar to real sunlight [71]. Xenon lamps emit black body radiation, and the colour temperature of xenon lamps is as high as 6000 K, which is very similar to that of the Sun [72]. Therefore, xenon lamps have been used in many PE photocatalytic degradation experimental studies due to the advantages mentioned above [73,74]. Based on the discussion above, the irradiation system was set as shown in Fig. 6. As shown in Fig. 6, the sample was placed under the xenon lamp, and the light ray was aligned with the crack.

2.8. Healing process

As mentioned earlier, the healing process starts if water enters mortar cracks. Therefore, the situation in which mortar cracks contact water and heal is simulated in this section. Under normal conditions, there can be various conditions through which water can enter mortar cracks, such as rain, snow, and hail. Among these conditions, rainy days are the most common situations and thus are simulated in this study. In the experiments, an automatic irrigation system used in agriculture was used to create simulated rainwater. A shower nozzle was suspended 5 cm above the crack to provide a gentle water stream. The water flow of the shower nozzle was 0.8 L/h. As shown in Fig. 7(a), many bubbles were generated in the cracks, and some even gushed out of the cracks when water went into them. According to Eqs. (1)–(8), bubbles should be generated from the chemical reaction of $NaHCO_3$ and $C_6H_8O_7$ and the reaction of Na_2CO_3 and $C_6H_8O_7$. We observed many bubbles being generated at the moment in which the automatic irrigation system was activated, which indicates that bubbles were formed by the direct reaction of a large number of reactants.

Since Na_2CO_3 is already a product of $NaHCO_3$ and $Ca(OH)_2$, the chemical reaction of $NaHCO_3$ and $C_6H_8O_7$ contributes mostly to the generation of initial bubbles rather than the reaction of Na_2CO_3 and $C_6H_8O_7$. Spraying lasted for 3 min, and the status of the mortar cracks after spraying is shown in Fig. 7(b). As shown in Fig. 7(b), most bubbles on the crack were washed out by water flow since the shower nozzle was pointed directly at the crack. Some bubbles around the crack still existed. Furthermore, a white substance could be observed to fill the crack. Theoretically, the white solid deposit filling the crack should be a mixture of insoluble materials such as $CaCO_3$ or $Ca_3(C_6H_5O_7)_2$. To clearly examine the materials filling the crack, the sample was dried at room temperature for 48 h to decrease all bubbles.

2.9. Healing results and water permeability tests

Fig. 8(a) and (b) and 8(c) show the healing results of samples containing one, two and three photocatalytic capsules, respectively. First, as seen in the three figures, the cracks are covered with white substances. The white substances look sticky and therefore stick to the mortar materials. The white substances do not have a regular appearance, which is expected because the healing process is spontaneous and uncontrolled. The distribution of repairing materials in the crack is formed by the random movements of bubbles. Second, the healing results in Fig. 8(b) and (c) are slightly better than those in Fig. 8(a). This indicates that more photocatalytic capsules will be helpful for the healing process, but the effect is limited.

Since a detailed conclusion cannot be obtained according to the observation, experimental studies were conducted to assess the different healing results. Since the mortar cracks investigated in this study are nonstructural cracks, mechanical properties are not considered, and the water permeability was selected as the experimental study to find differences between the different healing results. The water permeability was measured on both cracked and healed specimens. The tests were performed according to the study of Lv et al. [75]. The specimen surfaces were sealed with aluminium paper by waterproof glue, leaving only the crack mouth contacting water. Then, the specimen was placed into a container with the crack mouth facing up, as shown in Fig. 9. To ensure that there was no leakage for the following water permeability test, the edges of the samples were sealed with waterproof glue filled in the gap

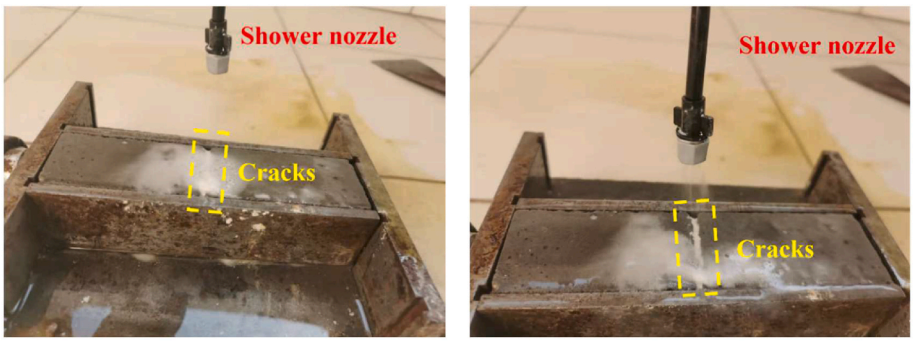

(a) (b)

Fig. 7. Cracks (a) at the beginning of spraying and (b) after 3 min of spraying.

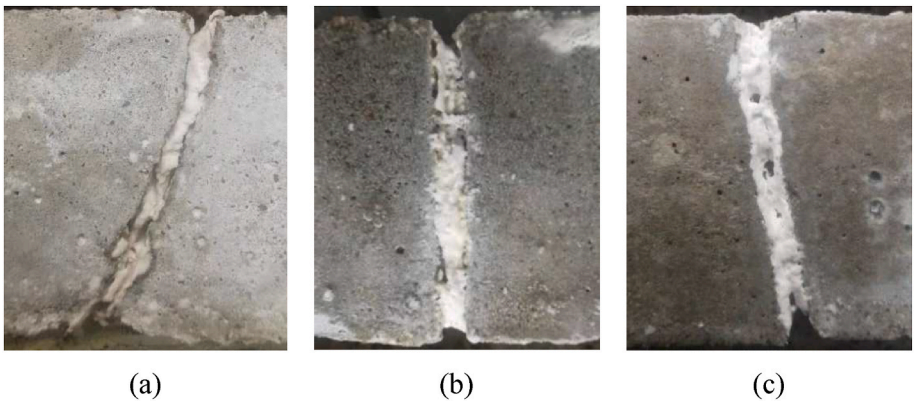

Fig. 8. Healing results with (a) one, (b) two, and (3) three capsules.

Fig. 9. Samples prepared for the water permeability tests.

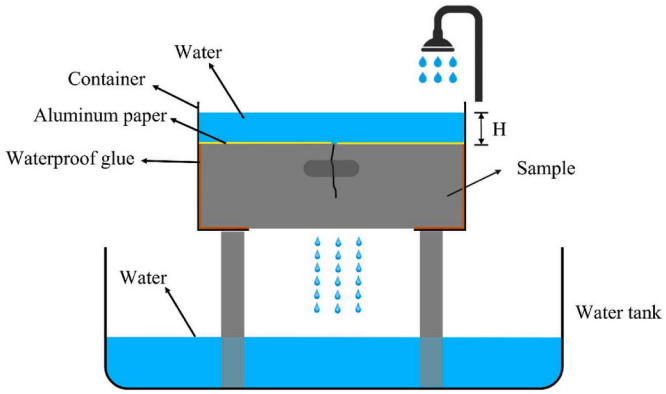

Fig. 10. Water permeability tests.

between the sample and container sides. The alphabetical order of the three samples in Fig. 9 corresponds to that in Fig. 8. Then, the sample was placed into a container. Water was added into the container quickly, and the height of water in the container was 5 cm, recorded as H. A water tank was placed under the container to contain water, as shown in Fig. 10. Finally, the weight of the water in the water tank was weighed and recorded every 2 min. The results of water permeability tests are

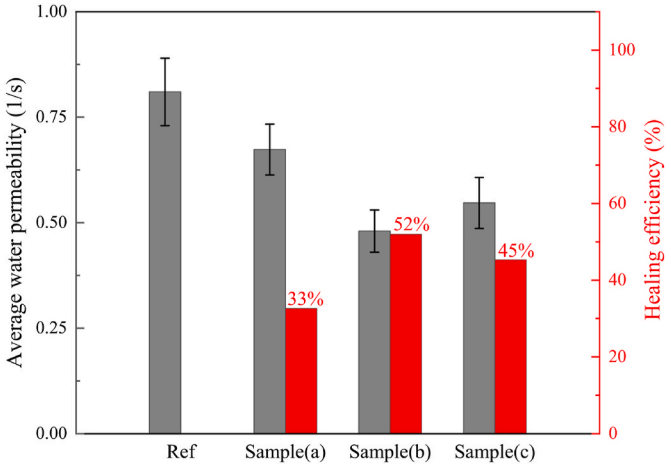

Fig. 11. Results of the average water permeabilities of the samples and healing. efficiencies based on the water permeability.

shown in Fig. 11.

The water permeability θ (1/s) was calculated according to Equation (23):

$$\theta = \frac{Q}{A \cdot H} \tag{23}$$

where Q is the flow of water through the cracks from the above to the below water tank. Q was defined as the volume increment of the out-flowed water per second, and the unit is cm^3/s. A is the area of the crack mouth, and H is the height of the water level on the mortar samples. Then, the healing efficiency is defined as follows:

$$\mu = (1 - \theta) \cdot 100\% \tag{24}$$

To eliminate the contingency of the experimental results, we

Table 4
One-way ANOVA of healing efficiency in terms of capsule number.

GROUPS	Healing efficiency			Mean value	Standard deviation	
Sample (a)	39%	32%	27%	33%	0.06028	
Sample (b)	57%	52%	47%	52%	0.05000	
Sample (c)	51%	46%	39%	45%	0.06028	
	DOF			Mean Square	F-ratio	p value
Between group	2			0.029	8.887	0.016
Within group	6			0.003		
Total	8					

Note: Samples (a), (b) and (c) contain one, two, and three capsules, respectively.

Table 5
One-way ANOVA of healing efficiency in terms of capsule number.

Comparison pairs		Mean difference	Standard deviation	p value
Sample (a)	Sample (b)	−0.19333	0.04659	0.006
	Sample (c)	−0.12667	0.04659	0.035
Sample (b)	Sample (a)	0.19333	0.04659	0.006
	Sample (c)	0.06667	0.04659	0.202
Sample (c)	Sample (a)	0.12667	0.04659	0.035
	Sample (b)	−0.06667	0.04659	0.202

repeated the process three times on one specimen and compared the results between cracked specimens and healed specimens.

Reference samples without healing treatment have the greatest water permeability (0.89/s), which is expected since microcracks exist in the gap between new-to-old mortars. The existence of microcracks has been confirmed by related studies [76,77]. As described in Section 2.6, the new mortar under the cracks was made after 21 days of curing of the sample. If water reaches the bottom of the cracks, it will continue to leak out through the microcracks. For sample (a) containing one capsule, the mean values of water permeability and standard deviation were 0.67/s and 0.06, respectively. For sample (b) and sample (c), the mean values of water permeability were 0.48/s and 0.55/s, and the standard deviations were 0.05 and 0.06, respectively. According to Eq. (24), the healing efficiencies of samples (a), (b) and (c) are 33%, 52% and 45%, respectively. Based on the above, a tentative conclusion is that self-healing by capsules should be effective and that the healing effects of 2 capsules and 3 capsules should be better than those of 1 capsule. However, similar to the observation results, more capsules are not necessarily better. Compared with sample (b) containing 2 capsules, the healing efficiency of sample (c) containing 3 capsules slightly decreased. To determine whether this result was statistically significant, one-way analysis of variance (one-way ANOVA) of healing efficiency was conducted. The number of capsules is the single variable in the one-way ANOVA. The one-way ANOVA results are shown in Tables 4 and 5.

Table 4 shows the one-way ANOVA results of the effect of the number of capsules on healing efficiency. There is a statistically significant difference in the healing efficiencies of the different numbers of capsules ($F = 15.76$, $p > 0.05$). Thus, the hypothesis in which there is a difference among the numbers of capsules can be accepted. However, the F test cannot provide information on whether there are significant differences among various combinations of groups, which means whether there is a statistical significance between samples (b) and (c) is still unknown. Hence, additional multiple comparisons that can indicate a significant relationship between particular pairs need to be performed for the groups. Here, the LSD method was used for multiple comparisons because the LSD method is the most-used method and has high accuracy.

As shown in Table 5, the healing efficiencies of both sample (b) and sample (c) were significantly different from the healing efficiency of sample (a) because the p values were 0.006 and 0.035, respectively. Based on the above, the healing effects of 2 capsules and 3 capsules are better than the healing effect of 1 capsule. However, there was no significant difference between the efficiencies of sample (b) and sample (c) (p value $= 0.202 > 0.05$). It is possible that the sample size included in the analysis was not large enough to obtain a significant result. Another reason might be that the healing efficiency of the three capsules is not necessarily better than that of the two capsules. We hypothesize that this may result from some holes on the surface of the repairing materials of sample (c). The holes on the sample surface increase the water permeability. If the reason why large-sized holes did not form in sample (a) and sample (b) needs to be given, it may be random. The disappearance of bubbles generated during the healing process is not uncontrolled and random. Based on the discussion above, some temporary conclusions can be obtained as follows. Basically, the increase in capsule number will bring more repairing materials, and hence, the healing efficiency will be better. However, the bubbles generated in the healing process increase the uncertainty of the healing results, which may make more capsules unable to bring better healing results.

3. Understanding the substances filling the concrete cracks by characterization methods

As previously described (Section 2.2), the products filling the cracks involve a variety of chemical reactions. These chemical reactions consist of various acid–base neutralization reactions and redox reactions. Since these chemical reactions were not performed in standard solution forms, we can hardly use redox chemistry to obtain the order of the various chemical reactions. It is also more likely that there is no clear order of the chemical reactions during the self-healing process. From the appearance of substances filling the crack exclusively, it is only known that cohesive white substances filled the cracks. This is not satisfied for the current observations. More detailed results need to be presented by further analysis to elucidate what exactly heals the cracks. Therefore, characterization technologies will be used to analyse the white substance filling the cracks.

First, from a materials science perspective, all substances are either crystalline, noncrystalline or a mixture of crystalline and noncrystalline. Cohesive white substances filling the cracks may contain unreacted $NaHCO_3$, $Ca(OH)_2$ and $C_6H_8O_7$, and these three materials were crystals purchased in the form of pure reagents. In addition, some products of Eqs. (1)–(8) may exist in the forms of crystals. Therefore, X-ray diffraction (XRD) technology was performed to find the existence of the crystal phases in the cohesive white substance filling the cracks.

Second, after determining the crystal phases in the repairing materials, we need to analyse the remaining noncrystalline phases. Since characterization technologies for crystal materials such as XRD are not available for later analysis, we decided to use scanning electron microscopy–energy dispersive spectrometry (SEM–EDS) to examine the surface morphology and elemental composition of the materials. With the results of SEM–EDS, the preliminary judgement for the noncrystalline phases could be confirmed. To increase confidence, transmission electron microscopy (TEM) will be used to verify the previous results according to the analysis of individual lattices. A schematic of the steps involved in the material characterization for the white substance filling the cracks is shown in Fig. 12.

3.1. Material characterization of products filling the cracks

3.1.1. XRD characterization of materials repairing the cracks

Fig. 13(a) and (b) show the XRD characterization of the powder from the interior and surfaces of the white substance, respectively. As shown in Fig. 13(a), three crystalline phases, $NaHCO_3$, $C_6H_8O_7$ and $Ca(OH)_2$, exist on the inner layer (internal surface) of the white substance filling the cracks, while there is only one crystalline phase, $Ca(OH)_2$, formed on the outer layer (external surface). This result shows that unreacted $Ca(OH)_2$ existed on the outer layer of the white substance filling the cracks, which is likely the reason for the generation of the viscosity of the white substance filling the cracks. We hypothesize that when the healing process started, part of the $Ca(OH)_2$ was not involved in the chemical reactions and was dissolved in water to possibly form a viscous lime slurry [78]. Lime slurry is a common adhesive and is widely used to fill the cracks of construction materials [78,79]. The lime slurry made the healing materials stick to the cracks, which helped repair materials combined with concrete better. Although the above result was not expected when we designed the self-healing mechanism, it is beneficial. In the next section, the existence of lime slurry is justified by the SEM results.

A possible reason for the disappearance of $NaHCO_3$ and $C_6H_8O_7$ on the outer layer of the sample is their property of being easily soluble in water [80,81]. The mortar sample was placed in an open environment so that water flow could wash out the dissolved $NaHCO_3$ and $C_6H_8O_7$. However, the situation is different for $Ca(OH)_2$. Lime slurry is not

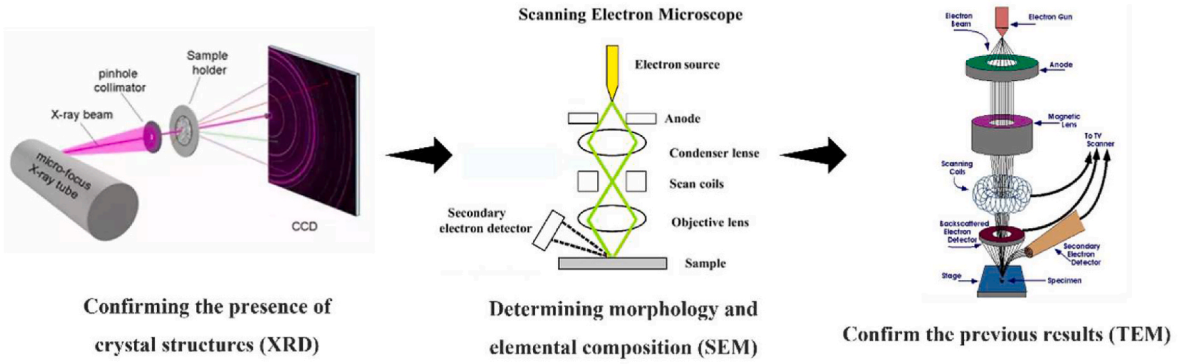

Fig. 12. Steps involved in material characterization for the white substance filling the cracks.

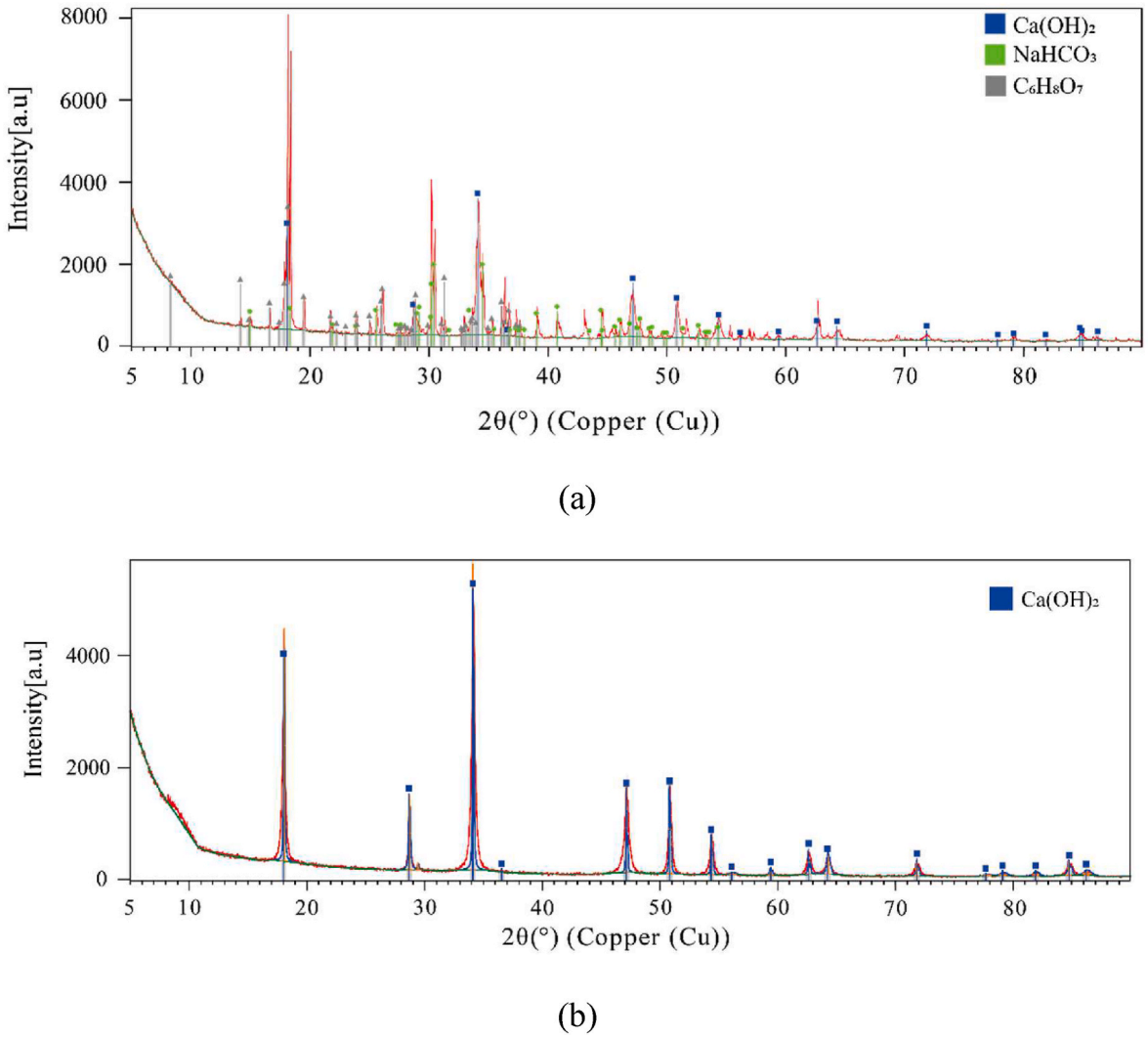

Fig. 13. XRD characterizations of the powder from (a) the inner layer and (b) outer layer of repairing materials.

actually soluble but consists of agglomerates of $Ca(OH)_2$ particles [82]. The lime slurry is left in the cracks because of its cohesion, and $Ca(OH)_2$ particles inside the agglomerates remain in a crystal phase. After evaporation of the free water between agglomerates, $Ca(OH)_2$ agglomerates solidify. If the solid $Ca(OH)_2$ agglomerates are ground into powder, its crystal structure is essentially the same as before. Thus, as seen in Fig. 13(a) and (b), the crystal structure of $Ca(OH)_2$ does not change.

Until now, detailed discussions about the XRD characterization of the powder from the white substance filling the cracks are given. Thus, the phenomenon of white substances sticking to the concrete can be well explained through the formation of $Ca(OH)_2$. However, the inner layer of white substances is not yet clear. It is only known that there are unreacted $NaHCO_3$, $C_6H_8O_7$ and $Ca(OH)_2$ in white substances filling the cracks. There are probably more details to be found. Therefore, the apparent morphology of the internal powder was observed directly by SEM to gain an intuitive and better understanding of the white substance

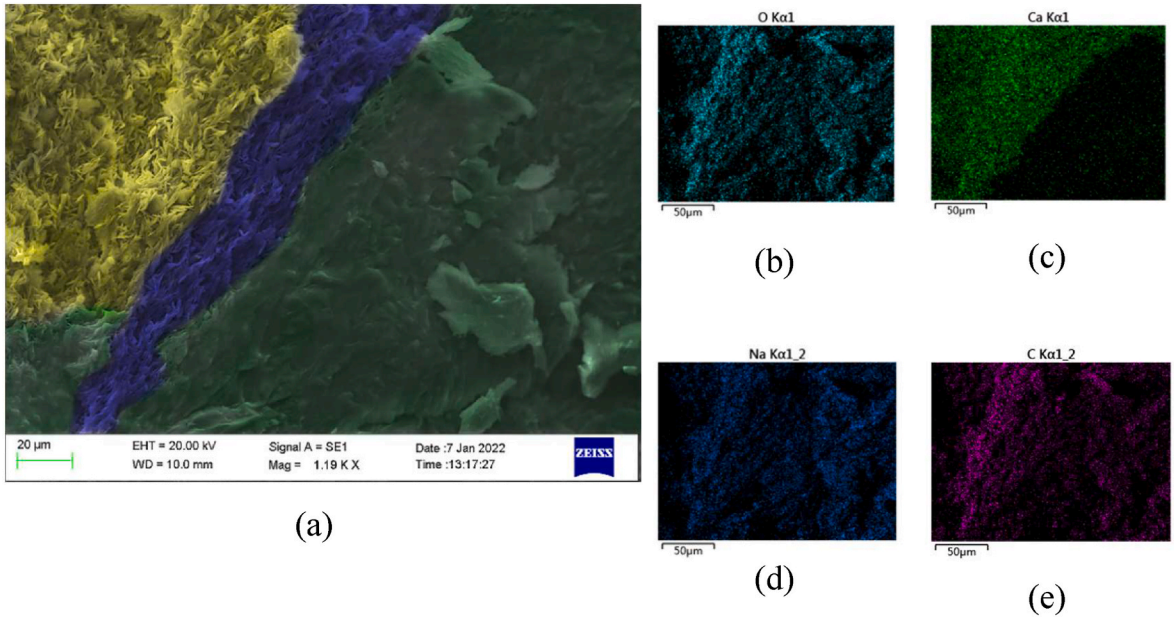

Fig. 14. SEM results.

filling the cracks.

3.1.2. SEM and TEM characterization of materials repairing the cracks

Although only $NaHCO_3$, $C_6H_8O_7$ and $Ca(OH)_2$ were detected by XRD, the repairing materials should consist of some other products of Eqs. (1)–(8), but they are not crystalline phases. Therefore, SEM characterization was performed for the materials filling the cracks. An approximately 2 mm × 2 mm × 2 mm piece was taken from the surface of the white substances filling the cracks for SEM characterization. After thorough investigation, a representative field was captured, as shown in Fig. 14(a), showing that three substances exhibiting different morphologies existed at the same time. The upper left part of Fig. 14(a) shows thin plate-shaped crystal clusters highlighted in yellow. According to the XRD results, the only crystalline material in the repaired materials is $Ca(OH)_2$, so the thin plate-shaped crystals should be $Ca(OH)_2$. Next, the right green part of Fig. 14(a) resembles the soluble substances that naturally evaporate to dryness. We hypothesize that this part may be dried $NaHCO_3$ or $C_6H_8O_7$ or even a mixture of $NaHCO_3$ and $C_6H_8O_7$. Between the yellow area and green area, there is a purple narrow band that should be $CaCO_3$ or $Ca_3(C_6H_5O_7)_2$. Below, we outline the reasoning behind this conjecture.

Since $Ca(OH)_2$ is slightly soluble in water, the crystal structure of most $Ca(OH)_2$ is not destroyed by the dissolution process. Correspondingly, thin plate-shaped $Ca(OH)_2$ crystals aggregate after drying and can still be observed in the form of crystals, which is consistent with Fig. 13 (a). Moreover, related literature [83,84] indicates that hexagonal crystals are the most common form of $Ca(OH)_2$ crystals and that $Ca(OH)_2$ reagents are essentially all in hexagonal crystal forms. Therefore, the substance located in the yellow area is agglomerated $Ca(OH)_2$. This also supports the hypothesis in the last section suggesting that lime slurry is generated in the white substances filling cracks because lime slurry is the suspension with agglomerated $Ca(OH)_2$ [85]. However, characteristics cannot be found for the morphology located in the right part of Fig. 14(a), where the EDS results can provide more details. As shown in Fig. 14(c), the calcium distribution has a significant characteristic in that most calcium concentrates in the yellow and purple areas, which indicates that the main substances in the green area do not contain calcium. Therefore, substances located in the green area should be $NaHCO_3$ or $C_6H_8O_7$ or a mixture of $NaHCO_3$ and $C_6H_8O_7$. In terms of why the green part does not have features of the crystal phase, the dissolution–precipitation process of $NaHCO_3$ or $C_6H_8O_7$ may change the crystal structures. According to the studies of Lu et al. [86,87], the structure of citric acid crystals will turn to an amorphous phase after dissolution–desiccation. In addition, according to the description of Post [88], the mixture of crystalline materials may cause the crystalline phase to not be identified. Therefore, crystal structures are not observed in the green area. As the substance in the yellow area is already $Ca(OH)_2$, the substances in the purple area are possibly insoluble calcium salts ($CaCO_3$ or $Ca_3(C_6H_5O_7)_2$) of Eqs. (1)–(8). There is an important statement supporting the conjecture that the purple area is precisely located between $Ca(OH)_2$ and the dried mixture of soluble substances of Eqs. (1)–(8). This is because $Ca(OH)_2$ contacts some substances, such as $C_6H_8O_7$ and $NaHCO_3$, which generates insoluble calcium salts. Moreover, the morphology of calcium carbonate in this study conforms to the calcium carbonate morphology generated by calcium hydroxide reported by related references [47,89,90].

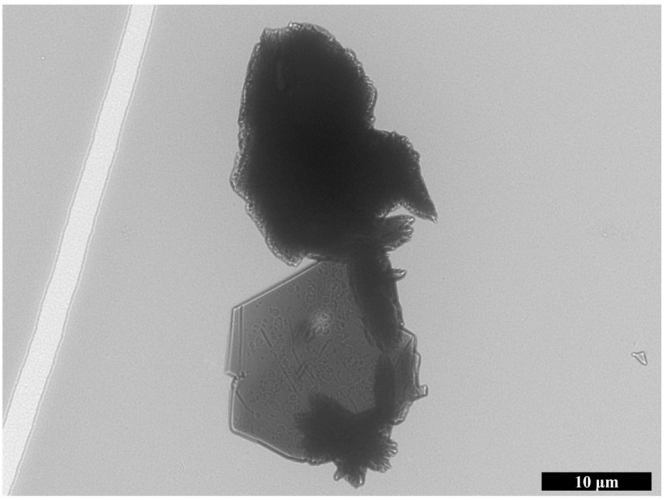

Fig. 15. TEM results showing calcium salt growing on a $Ca(OH)_2$ hexagonal grain.

Moreover, to provide more robust evidence of the results above, we performed TEM characterization. After multiple attempts, an image of calcium salt growing on $Ca(OH)_2$ grains was obtained, as shown in

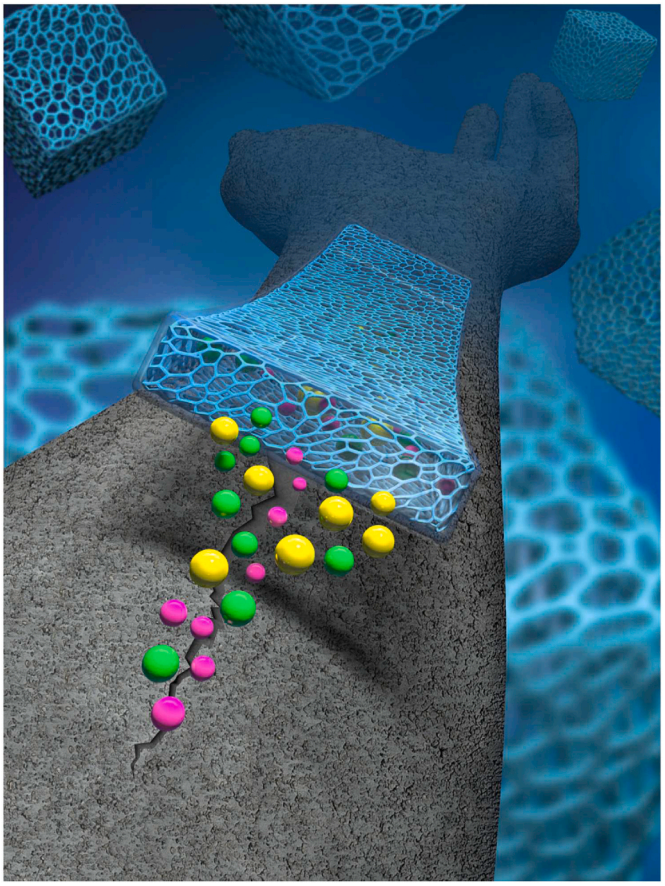

Fig. 16. Abstract schematic of repairing materials.

Fig. 15. As shown, a partly reacted hexagonal $Ca(OH)_2$ grain is placed at the bottom. Along the right edge of the grain, rod-like substances grow. The rod-like substance should be the calcium salt, which corresponds to the needle-like substance presented by yellow in Fig. 14(a). The TEM results of partly reacted hexagonal $Ca(OH)_2$ grains also support the XRD results showing that $NaHCO_3$, $C_6H_8O_7$ and $Ca(OH)_2$ do not react completely, and some $NaHCO_3$, $C_6H_8O_7$ and $Ca(OH)_2$ still exist in the form of crystals in the white substance filling the cracks. Furthermore, the remaining $Ca(OH)_2$ is able to continue to react with CO_2 to produce $CaCO_3$, as shown in Equation (7).

3.2. Analysis of the repairing materials

When $NaHCO_3$, $C_6H_8O_7$ and $Ca(OH)_2$ in the photocatalytic capsules contact water, they react rapidly and fill the cracks under the effect of generated CO_2 bubbles. Then, thin-layer insoluble calcium salt ($CaCO_3$ or $Ca_3(C_6H_5O_7)_2$) is generated on the surface of the mixture of $NaHCO_3$, $C_6H_8O_7$ and $Ca(OH)_2$. Soluble products may also be generated but will most likely be washed away by the water flow. At the same time, a portion of unreacted $Ca(OH)_2$ is mixed with water to form an adhesive lime slurry, which sticks to unreacted $NaHCO_3$, $C_6H_8O_7$, $Ca(OH)_2$ and all insoluble products above the cracks (as shown in Fig. 16). Under the thin layer of $CaCO_3$, unreacted $NaHCO_3$, $C_6H_8O_7$, and $Ca(OH)_2$ are buried. In addition, note that although there is unreacted $C_6H_8O_7$, which may be harmful to mortar considering it is a slightly corrosive substances [91], the neutralization of $NaHCO_3$ and $Ca(OH)_2$ can prevent the spread of citric acid in the mortar. Since the citric acid in the mortar is present in solid form, citric acid must rely on water to become a solution to leach into the surrounding matrix. However, $NaHCO_3$ and $Ca(OH)_2$ will react with citric acid immediately when water is provided. Therefore, there is no need to consider the corrosion effect of very little unreacted citric acid on mortar.

4. Insights, recommendations, and conclusions

In this paper, photocatalytic self-healing mortar, which can be healed by sunlight, was created by using photocatalytic capsules containing repairing materials. Then, the actual performance of the photocatalytic self-healing concrete was tested. The experiments indicate that it is feasible to use sunlight to heal the mortar. The photocatalytic capsules can be degraded by sunlight; therefore, the repairing materials are released to fill the cracks, and the healed mortar samples have waterproof properties. The final substances filling the cracks are insoluble calcium salts and unreacted $NaHCO_3$, $C_6H_8O_7$, and $Ca(OH)_2$.

Because the study is an unprecedented attempt to use sunlight to heal mortar, the experiments and characterizations of this study focus on the feasibility of the proposed method, and some points should be considered in the future:

(1) Sunlight: As the photocatalytic self-healing process is activated by sunlight energy, the conditions of sunlight should be considered. Simulated sunlight generated by a xenon lamp was confirmed to be effective in this study. Limited by experimental devices, the depth that sunlight reaches inside a crack cannot be determined at present.
(2) Capsule shells and photocatalysts: PE materials and the photocatalyst TiO_2 were used to make shells of photocatalytic capsules, and ideal results were obtained. With the rapid development of photocatalytic technology, more advanced photocatalysts and more environmentally friendly waterproof materials will be available in the future to make photocatalytic capsules.
(3) Repairing materials: $NaHCO_3$, $C_6H_8O_7$, and $Ca(OH)_2$ are not the only options for creating repairing materials. In fact, as long as insoluble and adhesive substances are generated, the healing process can be achieved theoretically. More alternative options could be tried in future studies.
(4) Healing results: The healing results of water permeability tests show that the function of bubbles generated in the healing process is a double-edged sword. Bubbles generated in the healing process can promote repairing materials filling the cracks but may leave holes on the surface of the repairing materials. Better methods to promote the repair of materials are awaited.
(5) Practical application: The photocatalytic capsules were applied during the hardening of mortar rather than mixing in this study. Therefore, the method proposed in this paper is suitable for concrete that can be used after casting, such as concrete pavement. The resistance of capsules for mechanical mixing needs to be further researched if they are to be applied from mixing.
(6) The follow-up situation of self-healing: Unreacted $Ca(OH)_2$ in concrete could bring more possibilities for any future healing process. For example, the healing product may benefit from the future long-term carbonization of $Ca(OH)_2$. The healing results might be improved after many rain cycles, which deserves much attention.

According to the description above, photocatalytic self-healing concrete requires further investigation. This challenges our current concepts and will energize the field of self-healing concrete and mortar.

Declaration of competing interest

The authors declare that they have no known competing financial interests or personal relationships that could have appeared to influence the work reported in this paper.

Data availability

Data will be made available on request.

Acknowledgements

This research was funded by the Key Special Project of “Science and Technology for Economy 2020" of China (Grant No. 2020YFB0312100ZL), National Natural Science Foundation of China (Grant No. 21976111), Shandong Provincial Natural Science Foundation (Grant No. ZR2019MB052) and ARC Discovery Projects (Grant No. DP210101425). We also thank Dr. Yue Li for inspiring our design idea for photocatalytic capsules.

References

[1] M. Shakoorioskooie, M. Griffa, A. Leemann, R. Zboray, P. Lura, Alkali-silica reaction products and cracks: X-ray micro-tomography-based analysis of their spatial-temporal evolution at a mesoscale, Cement Concr. Res. 150 (2021), 106593, https://doi.org/10.1016/j.cemconres.2021.106593.
[2] M.A. Hafiz, E. Denarié, Tensile response of UHPFRC under very low strain rates and low temperatures, Cement Concr. Res. 133 (2020), 106067, https://doi.org/10.1016/j.cemconres.2020.106067.
[3] J.-H. Jeong, N. Kim, Moisture effects on delamination and spalling distress mechanisms of early-age concrete pavements, KSCE J. Civ. Eng. 8 (2004) 197–204.
[4] M. Li, Multi-scale Design for Durable Repair of Concrete Structures, University of Michigan, 2009.
[5] M. Šahinagić–Isović, M. Ćećez, R. Radulović, Impact of Climate and Pollution on Resilience of Some Conventional Building Materials, Sustainable and Resilient Building Design 159.
[6] G. Yang, Y. Wu, H. Li, N. Gao, M. Jin, Z. Hu, J. Liu, Effect of shrinkage-reducing polycarboxylate admixture on cracking behavior of ultra-high strength mortar, Cem. Concr. Compos. 122 (2021), 104117, https://doi.org/10.1016/j.cemconcomp.2021.104117.
[7] A. James, E. Bazarchi, A.A. Chiniforush, P.P. Aghdam, M.R. Hosseini, A. Akbarnezhad, I. Martek, F. Ghodoosi, Rebar corrosion detection, protection, and rehabilitation of reinforced concrete structures in coastal environments: a review, Constr. Build. M-ater. 224 (2019) 1026–1039, https://doi.org/10.1016/j.conbuildmat.2019.07.250.
[8] F.U.A. Shaikh, Effect of cracking on corrosion of steel in concrete, Int. J. Concr. Struct. Mater. 12 (2018) 1–12, https://doi.org/10.1186/s40069-018-0234-y.
[9] V. Wiktor, H.M. Jonkers, Quantification of crack-healing in novel bacteria-based self-healing concrete, Cem. Concr. Compos. 33 (2011) 763–770, https://doi.org/10.1016/j.cemconcomp.2011.03.012.
[10] M.Z. Jumaat, M. Kabir, M. Obaydullah, A review of the repair of reinforced concrete beams, J. Appl. Sci. Res. 2 (2006) 317–326.
[11] M. Seifan, A.K. Samani, A. Berenjian, Bioconcrete: next generation of self-healing concrete, Appl. Microbiol. Biotechnol. 100 (2016) 2591–2602, https://doi.org/10.1007/s00253-016-7316-z.
[12] C. Schröfl, K.A. Erk, W. Siriwatwechakul, M. Wyrzykowski, D. Snoeck, Recent progress in superabsorbent polymers for concrete, Cement Concr. Res. 151 (2022), 106648, https://doi.org/10.1016/j.cemconres.2021.106648.
[13] D. Zhang, H. Wu, V.C. Li, B.R. Ellis, Autogenous healing of Engineered Cementitious Composites (ECC) based on MgO-fly ash binary system activated by carbonation curing, Construct. Build. Mater. 238 (2020), 117672, https://doi.org/10.1016/j.conbuildmat.2019.117672.
[14] G. Souradeep, H.W. Kua, Encapsulation technology and techniques in self-healing concrete, J. Mater. Civ. Eng. 28 (2016), 04016165, https://doi.org/10.1061/(ASCE)MT.1943-5533.0001687.
[15] W. Zhang, Q. Zheng, A. Ashour, B. Han, Self-healing cement concrete composites for resilient infrastructures: a review, Composites, Part B 189 (2020), 107892, https://doi.org/10.1016/j.compositesb.2020.107892.
[16] L.M. Mauludin, C. Oucif, Modeling of self-healing concrete: a review, Journal of Applied and Computational Mechanics 5 (2019) 526–539, https://doi.org/10.22055/JACM.2017.23665.1167.
[17] K. Van Tittelboom, N. De Belie, Self-healing in cementitious materials—a review, Materials 6 (2013) 2182–2217, https://doi.org/10.3390/ma6062182.
[18] C. Xue, W. Li, J. Li, V.W. Tam, G. Ye, A review study on encapsulation-based self-healing for cementitious materials, Struct. Concr. 20 (2019) 198–212, https://doi.org/10.1002/suco.201800177.
[19] M. Nakahata, Y. Takashima, H. Yamaguchi, A. Harada, Redox-responsive self-healing materials formed from host–guest polymers, Nat. Commun. 2 (2011) 1–6, https://doi.org/10.1038/ncomms1521.
[20] A. Vollpracht, B. Lothenbach, R. Snellings, J. Haufe, The pore solution of blended cements: a review, Mater. Struct. 49 (2016) 3341–3367, https://doi.org/10.1617/s11527-015-0724-1.
[21] A.C. Balazs, Modeling self-healing materials, Mater, Today Off. 10 (2007) 18–23, https://doi.org/10.1016/S1369-7021(07)70205-5.
[22] Y. Li, P. Hao, M. Zhang, Fabrication, characterization and assessment of the capsules containing rejuvenator for improving the self-healing performance of asphalt materials: a review, J. Clean. Prod. 287 (2021), 125079, https://doi.org/10.1016/j.jclepro.2020.125079.
[23] H. Pulikkalparambil, S. Siengchin, J. Parameswaranpillai, Corrosion protective self-healing epoxy resin coatings based on inhibitor and polymeric healing agents encapsulated in organic and inorganic micro and nanocontainers, Nano-Struct. Nano-Objects 16 (2018) 381–395, https://doi.org/10.1016/j.nanoso.2018.09.010.
[24] B. Blaiszik, M. Caruso, D. McIlroy, J. Moore, S. White, N. Sottos, Microcapsules filled with reactive solutions for self-healing materials, Polymer 50 (2009) 990–997, https://doi.org/10.1016/j.polymer.2008.12.040.
[25] T.D.P. Thao, T.J.S. Johnson, Q.S. Tong, P.S. Dai, Implementation of self-healing in concrete–proof of concept, IES J. Part A Civ. Struct. Eng. 2 (2009) 116–125, https://doi.org/10.1080/19373260902843506.
[26] N. Feng, H. Lin, H. Song, L. Yang, D. Tang, F. Deng, J. Ye, Efficient and selective photocatalytic CH4 conversion to CH3OH with O2 by controlling overoxidation on TiO2, Nat. Commun. 12 (2021) 1–10, https://doi.org/10.1038/s41467-021-24912-0.
[27] T.P. Yoon, M.A. Ischay, J. Du, Visible light photocatalysis as a greener approach to photochemical synthesis, Nat. Chem. 2 (2010) 527–532, https://doi.org/10.1038/nchem.687.
[28] A. Fujishima, K. Honda, Electrochemical photolysis of water at a semiconductor electrode, Nature 238 (1972) 37–38, https://doi.org/10.1038/238037a0.
[29] A.J. Esswein, D.G. Nocera, Hydrogen production by molecular photocatalysis, Chem. Rev. 107 (2007) 4022–4047, https://doi.org/10.1021/cr050193e.
[30] T.S. Teets, D.G. Nocera, Photocatalytic hydrogen production, Chem. Commun. 47 (2011) 9268–9274.
[31] J. Lasek, Y.-H. Yu, J.C. Wu, Removal of NOx by photocatalytic processes, J. Photochem. Photobiol., C 14 (2013) 29–52, https://doi.org/10.1016/j.jphotochemrev.2012.08.002.
[32] M. Ballari, M. Hunger, G. Hüsken, H. Brouwers, NOx photocatalytic degradation employing concrete pavement containing titanium dioxide, Appl. Catal., B 95 (2010) 245–254, https://doi.org/10.1016/j.apcatb.2010.01.002.
[33] Y. Zhou, M. Elchalakani, H. Liu, B. Briseghella, C. Sun, Photocatalytic concrete for degrading organic dyes in water, Environ. Sci. Pollut. Res. (2022) 1–14, https://doi.org/10.1007/s11356-021-18332-2.
[34] Y. Zhou, M. Elchalakani, P. Du, C. Sun, Cleaning up oil pollution in the ocean with photocatalytic concrete marine structures, J. Clean. Prod. 329 (2021), 129636, https://doi.org/10.1016/j.jclepro.2021.129636.
[35] A.M. Sescu, L. Favier, D. Lutic, N. Soto-Donoso, G. Ciobanu, M. Harja, TiO2 doped with noble metals as an efficient solution for the photodegradation of hazardous organic water pollutants at ambient conditions, Water 13 (2021) 19, https://doi.org/10.3390/w13010019.
[36] F. Lidia, H. Maria, TiO 2/fly ash nanocomposite for photodegradation of organic pollutant, in: Handbook of Nanomaterials and Nanocomposites for Energy and Environmental Applications, 2020, pp. 1–24, https://doi.org/10.1007/978-3-030-11155-7_11-1.
[37] Z. Liang, C.-F. Yan, S. Rtimi, J. Bandara, Piezoelectric materials for catalytic/photocatalytic removal of pollutants: recent advances and outlook, Appl. Catal., B 241 (2019) 256–269, https://doi.org/10.1016/j.apcatb.2018.09.028.
[38] O. Baghriche, S. Rtimi, C. Pulgarin, J. Kiwi, Polystyrene CuO/Cu2O uniform films inducing MB-degradation under sunlight, Catal. Today 284 (2017) 77–83, https://doi.org/10.1016/j.cattod.2016.10.018.
[39] X. Zhao, Z. Li, Y. Chen, L. Shi, Y. Zhu, Enhancement of photocatalytic degradation of polyethylene plastic with CuPc modified TiO2 photocatalyst under solar light irradiation, Appl. Surf. Sci. 254 (2008) 1825–1829, https://doi.org/10.1016/j.apsusc.2007.07.154.
[40] S. Li, S. Xu, L. He, F. Xu, Y. Wang, L. Zhang, Photocatalytic degradation of polyethylene plastic with polypyrrole/TiO2 nanocomposite as photocatalyst, Polymer Plastic. Technol. Eng. 49 (2010) 400–406, https://doi.org/10.1080/03602550903532166.
[41] W. Asghar, I.A. Qazi, H. Ilyas, A.A. Khan, M.A. Awan, M. Rizwan Aslam, Comparative solid phase photocatalytic degradation of polythene films with doped and undoped TiO2 nanoparticles, J. Nanomater. 2011 (2011), https://doi.org/10.1155/2011/461930.
[42] J. Xu, X. Wang, B. Wang, Biochemical process of ureolysis-based microbial CaCO3 precipitation and its application in self-healing concrete, Appl. Microbiol. Biotechnol. 102 (2018) 3121–3132, https://doi.org/10.1007/s00253-018-8779-x.
[43] S. Choi, S. Park, M. Park, Y. Kim, K.M. Lee, O.-M. Lee, H.-J. Son, Characterization of a novel CaCO3-forming alkali-tolerant rhodococcus erythreus S26 as a filling agent for repairing concrete cracks, Molecules 26 (2021) 2967, https://doi.org/10.3390/molecules26102967.
[44] Y.Ç. Erşan, H. Verbruggen, I. De Graeve, W. Verstraete, N. De Belie, N. Boon, Nitrate reducing CaCO3 precipitating bacteria survive in mortar and inhibit steel corrosion, Cement Concr. Res. 83 (2016) 19–30.
[45] C. Liu, X. Xu, Z. Lv, L. Xing, Self-healing of concrete cracks by immobilizing microorganisms in recycled aggregate, J. Adv. Concr. Technol. 18 (2020) 168–178, https://doi.org/10.3151/jact.18.168.
[46] M. Alexander, A. Bertron, N. De Belie, Performance of Cement-Based Materials in Aggressive Aqueous Environments, Springer, 2013, https://doi.org/10.1007/978-94-007-5413-3.
[47] M. Rao, V.S. Reddy, M. Hafsa, P. Veena, P. Anusha, Bioengineered concrete-a sustainable self-healing construction material, Res. J. Eng. Sci. ISSN 2278 (2013) 9472.
[48] K. Pappupreethi, R. Ammakunnoth, P. Magudeaswaran, Bacterial concrete: a review, Int. J. Civ. Eng. Technol. 8 (2017) 588–594.
[49] J. Wang, A. Mignon, D. Snoeck, V. Wiktor, S. Van Vliergerghe, N. Boon, N. De Belie, Application of modified-alginate encapsulated carbonate producing bacteria

in concrete: a promising strategy for crack self-healing, Front. Microbiol. 6 (2015) 1088, https://doi.org/10.3389/fmicb.2015.01088.
[50] S. Gupta, S. Dai Pang, H.W. Kua, Autonomous healing in concrete by bio-based healing agents–A review, Construct. Build. Mater. 146 (2017) 419–428, https://doi.org/10.1016/j.conbuildmat.2017.04.111.
[51] C. USP, The United States pharmacopeia, Nat. Formul. 14 (2008).
[52] W.W. Porterfield, Inorganic Chemistry, Academic press, 2013.
[53] N. Dasgupta, C. Chen, A.C. van Duin, Development and application of ReaxFF methodology for understanding the chemical dynamics of metal carbonates in aqueous solutions, Phys. Chem. Chem. Phys. (2022), https://doi.org/10.1039/D1CP04790F.
[54] N. Liu, N. Lu, H. Yu, S. Chen, X. Quan, Enhanced degradation of organic water pollutants by photocatalytic in-situ activation of sulfate based on Z-scheme g-C3N4/B- iPO4, Chem. Eng. J. 428 (2022), 132116, https://doi.org/10.1016/j.cej.2021.132116.
[55] A. Shafi, S. Bano, L. Sharma, A. Halder, S. Sabir, M.Z. Khan, Exploring multifunctional behaviour of g-C3N4 decorated BiVO4/Ag2CO3 hierarchical nanocomposite for simultaneous electrochemical detection of two nitroaromatic compounds and water splitting applications, Talanta (2022), 123257, https://doi.org/10.1016/j.talanta.2022.123257.
[56] M. Náfrádi, T. Alapi, G. Bencsik, C. Janáky, Impact of reaction parameters and water matrices on the removal of organic pollutants by TiO2/LED and ZnO/LED heterogeneous photocatalysis using 365 and 398 nm radiation, Nanomaterials 12 (2022) 5, https://doi.org/10.3390/nano12010005.
[57] S.J. Liu, C.H. Yang, Rotational molding of two-layered polyethylene foams, Adv. Polym. Technol.: J. Polymer. Process Insitute. 20 (2001) 108–115, https://doi.org/10.1002/adv.1008.
[58] A.R. Cowan, C.M. Costanzo, R. Benham, E.J. Loveridge, S.C. Moody, Fungal bioremediation of polyethylene: challenges and perspectives, J. Appl. Microbiol. 132 (2022) 78–89, https://doi.org/10.1111/jam.15203.
[59] Y. Guo, P. Zhang, H. Ding, C. Le, Experimental study on the permeability of SAP modified concrete, Materials 13 (2020) 3368, https://doi.org/10.3390/ma13153368.
[60] R.E. Pease, Hydraulic Properties of Asphalt Concrete, The University of New Mexico, 2010.
[61] W. Liang, Y. Luo, S. Song, X. Dong, X. Yu, High photocatalytic degradation activity of polyethylene containing polyacrylamide grafted TiO2, Polym. Degrad. Stabil. 98 (2013) 1754–1761, https://doi.org/10.1016/j.polymdegradstab.2013.05.027.
[62] D.A. Maulana, M. Ibadurrohman, Synthesis of nano-composite Ag/TiO2 for polyethylene microplastic degradation applications, in: IOP Conf. Ser.: Mater. Sci. Eng., IOP Publishing, 2021, 012054, https://doi.org/10.1088/1757-899X/1011/1/012054.
[63] X. u Zhao, Z. Li, Y. Chen, L. Shi, Y. Zhu, Solid-phase photocatalytic degradation of polyethylene plastic under UV and solar light irradiation, J. Mol. Catal. Chem. 268 (2007) 101–106, https://doi.org/10.1016/j.molcata.2006.12.012.
[64] W.L.N. Bandara, R.M. de Silva, K.N. de Silva, D. Dahanayake, S. Gunasekara, K. Thanabalasingam, Is nano ZrO2 a better photocatalyst than nano TiO2 for degradation of plastics? RSC Adv. 7 (2017) 46155–46163, https://doi.org/10.1039/C7RA08324F.
[65] L. Zan, W. Fa, S. Wang, Novel photodegradable low-density polyethylene– TiO2 nanocomposite film, Environ. Sci. Technol. 40 (2006) 1681–1685, https://doi.org/10.1021/es051173x.
[66] K. Van Tittelboom, J. Wang, M. Araújo, D. Snoeck, E. Gruyaert, B. Debbaut, H. Derluyn, V. Cnudde, E. Tsangouri, D. Van Hemelrijck, Comparison of different approaches for self-healing concrete in a large-scale lab test, Construct. Build. Mater. 107 (2016) 125–137, https://doi.org/10.1016/j.conbuildmat.2015.12.186.
[67] J. Feiteira, E. Tsangouri, E. Gruyaert, C. Lors, G. Louis, N. De Belie, Monitoring crack movement in polymer-based self-healing concrete through digital image correlation, acoustic emission analysis and SEM in-situ loading, Mater. Des. 115 (2017) 238–246, https://doi.org/10.1016/j.matdes.2016.11.050.
[68] M. Araújo, S. Chatrabhuti, S. Gurdebeke, N. Alderete, K. Van Tittelboom, J.-M. Raquez, V. Cnudde, S. Van Vlierberghe, N. De Belie, E. Gruyaert, Poly (methyl methacrylate) capsules as an alternative to the ‘’proof-of-concept’’glass capsules used in self-healing concrete, Cem. Concr. Compos. 89 (2018) 260–271, https://doi.org/10.1016/j.cemconcomp.2018.02.015.
[69] P. Nama, A. Jain, R. Srivastava, Y. Bhatia, Study on causes of cracks & its preventive measures in concrete structures, Int. J. Eng. Res. Afr. 5 (2015) 119–123.
[70] P.S. Barve, L.S. Thakur, R.P. Barve, J.K. Shah, N.P. Patel, Detection and sizing study of cracks: a case study, Int. J. Adv. Res. Eng. Sci. Technol. 2 (2015) 84–91.
[71] J.J.J.F. Randall, Is AM1.5 applicable in practice? Modelling eight photovoltaic materials with respect to light intensity and two spectra, Renew. Energy 28 (2003) 1851–1864, https://doi.org/10.1016/S0960-1481(03)00068-5.
[72] J. Miyake, S. Kawamura, Efficiency of light energy conversion to hydrogen by the photosynthetic bacterium Rhodobacter sphaeroides, Int. J. Hydrogen Energy 12 (1987) 147–149, https://doi.org/10.1016/0360-3199(87)90146-7.
[73] Y. Zhao, F. Zhang, J. Zhang, K. Zou, J. Zhang, C. Chen, M. Long, Q. Zhang, J. Wang, C. Zheng, Preparation of composite photocatalyst with tunable and self-indicating delayed onset of performance and its application in polyethylene degradation, Appl. Catal., B 286 (2021), 119918, https://doi.org/10.1016/j.apcatb.2021.119918.
[74] M. Romero-Sáez, L. Jaramillo, R. Saravanan, N. Benito, E. Pabón, E. Mosquera, F. Gracia, Notable photocatalytic activity of TiO2-polyethylene nanocomposites for visible light degradation of organic pollutants, Express Polym. Lett. 11 (2017) 899–909, https://doi.org/10.3144/expresspolymlett.2017.86.
[75] L. Lv, P. Guo, G. Liu, N. Han, F. Xing, Light induced self-healing in concrete using novel cementitious capsules containing UV curable adhesive, Cem. Concr. Compos. 105 (2020), 103445, https://doi.org/10.1016/j.cemconcomp.2019.103445.
[76] Y. He, X. Zhang, R. Hooton, X. Zhang, Effects of interface roughness and interface adhesion on new-to-old concrete bonding, Construct. Build. Mater. 151 (2017) 582–590, https://doi.org/10.1016/j.conbuildmat.2017.05.049.
[77] S. Feng, H. Xiao, R. Liu, X. Dong, Z. Liu, H. Liu, The influence of different bond primers on the bond strength of concrete overlays and the microstructure of the overlays transition zone, Cem. Concr. Compos. 119 (2021), 104023, https://doi.org/10.1016/j.cemconcomp.2021.104023.
[78] Y.-R. Kim, J.S. Lutif, A. Bhasin, D.N. Little, Evaluation of moisture damage mechanisms and effects of hydrated lime in asphalt mixtures through measurements of mixture component properties and performance testing, J. Mater. Civ. Eng. 20 (2008) 659–667, https://doi.org/10.1061/(ASCE)0899-1561 (2008) 20:10(659).
[79] A. Pasandín, I. Pérez, B. Gómez-Meijide, N. Pérez-Barge, The effect of hydrated lime on the bond between asphalt and recycled concrete aggregates, Petrol. Sci. Technol. 33 (2015) 1141–1148, https://doi.org/10.1080/10916466.2014.984076.
[80] M. Drogowska, L. Brossard, H. Menard, Copper dissolution in NaHCO3 and NaHCO3+ NaCl aqueous solutions at pH 8, J. Electrochem. Soc. 139 (1992) 39.
[81] J. Wu, Z.-C. Xu, J.-X. Chen, L. He, Wet etching for InAs-based InAs/Ga (As) Sb superlattice long wavelength infrared detectors, J. Infrared Millim. Waves 38 (2019), https://doi.org/10.11972/j.issn.1001-9014.2019.05.001.
[82] Y. Wang, Z. Xu, J. Wang, Z. Zhou, P. Du, X. Cheng, Synergistic effect of nano-silica and silica fume on hydration properties of cement-based materials, J. Therm. Anal. Calorim. 140 (2020) 2225–2235, https://doi.org/10.1007/s10973-019-08929-8.
[83] C.R. Theocharis, Functionalisation of the surface of calcium hydroxide by grafting of organic molecules, Mol. Cryst. Liq. Cryst. 187 (1990) 345–350, https://doi.org/10.1080/00268949008036060.
[84] D.K. Chanda, P. Khan, N. Dey, M. Majumder, A.K. Chakraborty, B.B. Jha, J. Ghosh, Synthesis of calcium based nano powders for application in conservation and restoration of heritage mortar, SN Appl. Sci. 2 (2020) 1–11, https://doi.org/10.1007/s42452-020-2138-0.
[85] F.A. Cardoso, H.C. Fernandes, R.G. Pileggi, M.A. Cincotto, V.M. John, Carbide lime and industrial hydrated lime characterization, Powder Technol. 195 (2009) 143–149, https://doi.org/10.1016/j.powtec.2009.05.017.
[86] Q. Lu, G. Zografi, Phase behavior of binary and ternary amorphous mixtures containing indomethacin, citric acid, and PVP, Pharm. Res. (N. Y.) 15 (1998) 1202–1206, https://doi.org/10.1023/A:1011983606606.
[87] Q. Lu, G. Zografi, Properties of citric acid at the glass transition, J. Pharmacol. Sci. 86 (1997) 1374–1378, https://doi.org/10.1021/js970157y.
[88] J.E. Post, Manganese oxide minerals: crystal structures and economic and environmental significance, Proc. Natl. Acad. Sci. USA 96 (1999) 3447–3454, https://doi.org/10.1073/pnas.96.7.3447.
[89] H. Tang, J. Yu, X. Zhao, Controlled synthesis of crystalline calcium carbonate aggregates with unusual morphologies involving the phase transformation from amorphous calcium carbonate, Mater. Res. Bull. 44 (2009) 831–835, https://doi.org/10.1016/j.materresbull.2008.09.002.
[90] G. Xing, L. Zhang, W. Xuan, Y. Pan, Y. Zhao, B. Zhang, Influence of alkaline activators on unconfined compressive strength of saline soils stabilised with ground granulated blast furnace slags, Adv. Civ. Eng. 2021 (2021), https://doi.org/10.1155/2021/8893106.
[91] E. Cuenca, L. D'Ambrosio, D. Lizunov, A. Tretjakov, O. Volobujeva, L. Ferrara, Mechanical properties and self-healing capacity of ultra high performance fibre reinforced concrete with alumina nano-fibres: tailoring ultra high durability concrete for aggressive exposure scenarios, Cem. Concr. Compos. 118 (2021), 103956, https://doi.org/10.1016/j.cemconcomp.2021.103956.